

## Numerical modelling and analysis of earth abundant $Sb_2S_3$ and $Sb_2Se_3$ based solar cells using SCAPS-1D

Arindam Basak, Udai P. Singh\*

*Thin Film Photovoltaic Lab, School of Electronics Engineering, KIIT- Deemed to be University, Bhubaneswar, 751024, Odisha, India*



### ARTICLE INFO

**Keywords:**  
Simulation  
 $Sb_2S_3$  and  $Sb_2Se_3$  solar cell  
Optimization  
Work function  
I-V, C-V measurement

### ABSTRACT

Antimony chalcogenides,  $Sb_2S_3$  and  $Sb_2Se_3$ , are the promising candidates for next generation solar cells due to its non-toxicity, earth abundance, low cost and easy availability. In this work,  $Sb_2S_3$  and  $Sb_2Se_3$  hetero-junction solar cells are modeled, numerically analyzed and compared by the SCAPS (Solar Cell Capacitance Simulator) software. Initial simulation for configuration optimization was done in detail for absorber layer thickness, buffer layer thickness, acceptor density, radiative recombination coefficient, series-shunt resistance, defect density and the work function of the back contact. A detailed analysis of the junction characteristics like carrier generation and recombination, built-in electric field and capacitance-voltage (C-V) study was also done in the second stage to determine the carrier lifetime, depletion width, built-in potential and doping density.

The present study shows that, the optimum thickness for  $Sb_2S_3$  absorber layer is  $2.5\ \mu m$  and for  $Sb_2Se_3$  absorber layer is  $2\ \mu m$  to achieve the best efficiency. The buffer layer optimum thickness for  $Sb_2S_3$  and  $Sb_2Se_3$  solar cell is in the range of  $50\ nm$  to  $60\ nm$ . The optimum series and shunt resistance for  $Sb_2S_3$  and  $Sb_2Se_3$  based solar cell device is coming in the range of  $3-5\ \Omega\cdot cm^2$  and  $300-450\ \Omega\cdot cm^2$  respectively. It is also found that metal having work function  $5eV$  or more is better to be used as an electrode in  $Sb_2S_3$  or  $Sb_2Se_3$  based solar cell. A maximum efficiency of  $9.51\%$  and  $12.62\%$  is achieved after optimizing different parameters for the  $Sb_2S_3$  and  $Sb_2Se_3$  solar cells respectively.

### 1. Introduction

For the last few years, thin film solar cell technology is gaining interest among the research community mainly due to CIGS and CdTe solar cells, having efficiency more than  $20\%$  [1]. The low abundance of In and Te, toxicity of Cd are the main limitations of using these compound semiconductors as an absorber layer for solar cell [2]. As a replacement, new materials like CZTS, CTS, SnS,  $Sb_2S_3$ ,  $Sb_2Se_3$  are proposed and studied as absorber material for thin film solar cells. These semiconductors have the advantages like p-type conductivity, high absorption coefficient, suitable direct bandgap to be used as an thin film absorber layer material. Among these, CZTS is the most researched material and obtained efficiency of  $12.6\%$ , but defects, appearance of secondary phases, phase complexity are the major bottlenecks for this material to improve its efficiency. For the last five years, no enhancement of efficiency is achieved. So the research community is concentrating now on other binary materials which actually showing improved performance in terms of solar cell efficiency [3,4].

Thin film antimony chalcogenides based solar cells recently

appearing as an emerging topic of interest among the researchers.  $Sb_2S_3$  and  $Sb_2Se_3$ , V-VI semiconductor, possess excellent opto-electrical properties like high absorption coefficient ( $>10^5\ cm^{-1}$ ), tunable bandgap ( $1.04-1.67\ eV$ ), intrinsic p-type conductivity, decent carrier mobility ( $9-15\ cm^2/V.s$ ), low toxicity, moisture and air stability [5,6]. Hence, these materials are very much suitable for the application in various opto-electronic fields. Apart from the above advantages, these materials have other added advantages like earth abundance, less structural complexity, less appearance of other secondary phases and low melting point [7].

$Sb_2S_3$  and  $Sb_2Se_3$  solar cells were deposited by various deposition techniques, like chemical bath deposition [8], sputtering [9], thermal evaporation [10,11], atomic layer deposition [12] etc. Efforts are still going on to modify the device efficiency by using different deposition routes and optimizing its parameters. Recent studies show that,  $Sb_2S_3$  and  $Sb_2Se_3$  obtained considerable momentum in its research and achieved record efficiency of  $7.5\%$  and  $9.2\%$  respectively. Solar cells based on  $Sb_2Se_3$  layers deposited by Closed Space Sublimation (CSS) is very close to cross the  $10\%$  efficiency benchmark [13,14]. Though the

\* Corresponding author.

E-mail address: [singhup@kiit.ac.in](mailto:singhup@kiit.ac.in) (U.P. Singh).

research is concentrating on its promising aspects of improvement in efficiency, in actual it is still behind the Shockley-Queisser (S-Q) limit of efficiency and also far lower than the reported efficiency of CdTe and CIGS solar cells [15]. According to some recent studies, the main obstacle in obtaining high efficiency for antimony chalcogenide based solar cell are non-ideal series and shunt resistance, deep defects, non-radiative and interface recombination, inter-diffusion between layers etc. Due to these bottlenecks the obtained  $V_{oc}$  is quite less than the S-Q limit [16]. Now to study the effect of these defects and to optimize it, a proper numerical analysis is required for antimony chalcogenides ( $Sb_2S_3$  and  $Sb_2Se_3$ ) based solar cells. Several researchers have worked on different device optimization parameters of  $Sb_2S_3$  and  $Sb_2Se_3$  solar cells separately [11,17,18]. Till now not a single research article is available which studied the effect of different device parameters and defect on the  $Sb_2S_3$  and  $Sb_2Se_3$  solar cell concurrently and did a detailed comparative analysis on the impact of these parameters on the both types of solar cell. Also the in-depth analysis of the p-n junctions characteristics are very rare in the simulation studies.

In this work, the configuration used for the  $Sb_2S_3$  and  $Sb_2Se_3$  solar cell device structure was Mo/( $Sb_2S_3$  or  $Sb_2Se_3$ )/CdS/i-ZnO/ZnO:Al/metal contact. The device modeling and optimization was done in two steps. In the first step, the device parameters like, absorber layer and buffer layer thickness, acceptor density, radiative recombination coefficient, defect density of the absorber layer, series and shunt resistance of the total device and the work function of back contact was optimized. In the second step, after optimizing all the parameters, junction characteristics like carrier generation and recombination, built in electric field and the C-V characteristics of the device was studied to get a detailed insight of the device junction parameters which will help to understand the shortcomings of the  $Sb_2S_3$  and  $Sb_2Se_3$  based thin film solar cells and the impact of different solar cell parameters on its efficiency.

## 2. Device structure and simulation methodology

### 2.1. Device structure

The proposed device structure used for this simulation study is Mo/( $Sb_2S_3$  or  $Sb_2Se_3$ )/CdS/i-ZnO/ZnO:Al/metal contact and shown in Fig. 1, where Molybdenum (Mo) is a back contact,  $Sb_2S_3$  or  $Sb_2Se_3$  is absorber layer, CdS is wide bandgap window layer. Next to the buffer layer, highly resistive i-ZnO layer was used which is overlaid with Al doped ZnO (ZnO:Al) layer used as a transparent conductive oxide (TCO) to collect and carry charges out of the cell. The role of the i-ZnO layer is to restrict the intermixing between the absorber and TCO layer which in turn reduced the shunting pathways. Mo is used to collect the generated charges and works as a positive pole of the solar cell [19].

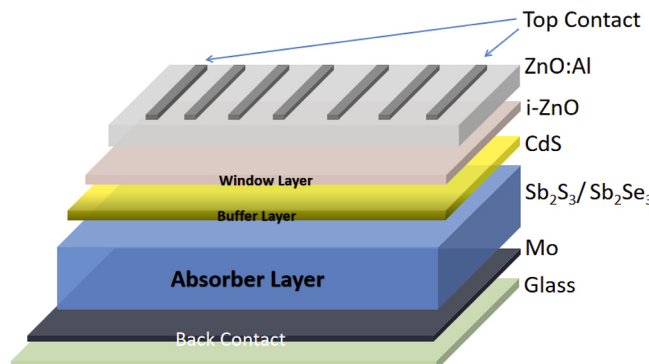


Fig. 1. Schematic diagram of the proposed structure.

### 2.2. SCAPS-1D simulation methodology

A number of software are available which are used by several researchers to explore the performance of TFSCs like AMPS [20], SILVACO ATLAS [21], COMSOL [22], wxAMPS [23], and SCAPS [24]. In our present study we have used SCAPS (Version 3.3.07) which is a one-dimensional, window based solar cell simulator, developed by Department of Electronics and Information Systems of the Gent University, Belgium to simulate the performance of solar cell and its various determining parameters. The SCAPS software have several advantages like, performance analysis can be done up to seven different layers, with several in-depth and batch analysis, easy to learn and interpret the obtained results [25]. In addition, the results obtained from SCAPS simulator have good agreement with the existing experimental results as reported by other researchers. Recently a number of research articles have been published on SCAPS-1D software exploring its application in finding efficiencies of different types of solar cell [26–28].

The analysis of SCAPS-1D is based upon Poisson's equation, hole continuity, electron continuity as given below [29]:

$$\frac{\partial^2 \Psi}{\partial x^2} + \frac{q}{\epsilon} [p(x) - n(x) + N_D - N_A + \rho_p - \rho_n] = 0 \quad (1)$$

$$\frac{1}{q} \frac{dJ_p}{dx} = G_{op}(x) - R(x) \quad (2)$$

$$\frac{1}{q} \frac{dJ_n}{dx} = -G_{op}(x) + R(x) \quad (3)$$

Where,  $\epsilon$  is the dielectric constant,  $q$  is the electron charge,  $N_A$  and  $N_D$  are acceptor and donor type density respectively,  $\Psi$  is the electrostatic potential,  $p$ ,  $n$ ,  $\rho_p$ ,  $\rho_n$ ,  $J_p$ ,  $J_n$  are hole concentration, electron concentration, hole distribution, electron distribution, current densities of hole and current densities of electron respectively.  $G_{op}$  is the optical generation rate,  $R$  is the net recombination from direct and indirect recombination. All of these parameters are the function of the position coordinate  $x$ .

For the simulation of device structure using SCAPS-1D software several material parameters need to be included in each layer of the structure. Table 1 represents all the material parameters used for the simulation study. All these parameters are extracted from other literature [19,30]. For all simulation study, the illumination used was AM 1.5 spectrum, 1000 W/m<sup>2</sup> from the front side.

Table 1  
Materials parameters used in the simulation.

Material Properties	ZnO:Al	i-ZnO	CdS	$Sb_2S_3$	$Sb_2Se_3$
Thickness (nm)	200	50	50–60	Variable	Variable
Bandgap (eV)	3.3	3.3	2.4	1.62	1.08
Electron Affinity (eV)	4.4	4.5	4.2	3.7	3.7
Dielectric Permittivity	9	9	10	7.08	9.86
CB Effective Density of State (1/cm <sup>3</sup> )	$2.2 \times 10^{18}$	$2.2 \times 10^{18}$	$2.2 \times 10^{18}$	$20 \times 10^{18}$	$18 \times 10^{18}$
VB Effective Density of State (1/cm <sup>3</sup> )	$1.8 \times 10^{19}$	$1.8 \times 10^{19}$	$10^{19}$	$10^{18}$	$10^{18}$
Electron Thermal Velocity (cm/s)	$10^7$	$10^7$	$10^7$	$10^7$	$10^7$
Hole Thermal Velocity (cm/s)	$10^7$	$10^7$	$10^7$	$10^7$	$10^7$
Electron Mobility (cm <sup>2</sup> /V.s)	$10^2$	$10^2$	$10^2$	9.8	15
Hole Mobility (cm <sup>2</sup> /V.s)	25	25	25	10	5.1
Donor Density ( $N_D$ cm <sup>-3</sup> )	$10^{20}$	$10^{18}$	$1.1 \times 10^{17}$	0	0
Acceptor Density ( $N_A$ cm <sup>-3</sup> )	0	$10^{18}$	0	$5.7 \times 10^{15}$	$5 \times 10^{15}$

### 3. Results and discussion

The major focus of this research work is to study the effect of different parameters of absorber layer on the photo conversion efficiency of solar cell and also to compare the effect of the same parameter for  $\text{Sb}_2\text{S}_3$  and  $\text{Sb}_2\text{Se}_3$  based thin film solar cells. Implementation of the optimized data will enable us to fix a set of criteria for real time design of solar photovoltaic device with an optimum efficiency.

The modelling and the simulation study were done in two steps. In the first stage of optimization, (a) the thickness of  $\text{Sb}_2\text{S}_3$  and  $\text{Sb}_2\text{Se}_3$  (b) the thickness of CdS buffer layer (c) recombination density, defect density, carrier density (d) series and shunt resistance of the device (e) work function of the back contact was optimized.

After optimizing the above parameters, the optimized data was used to further examine the junction and other device parameters using C-V characteristic study, carrier generation and recombination study and built-in electric field generation. This in-depth study enable us to find the shortcomings of the  $\text{Sb}_2\text{S}_3$  and  $\text{Sb}_2\text{Se}_3$  based thin film solar cell which in turn will lead the research community to find more efficient solar cell device.

#### 3.1. Effect of thickness of absorber layer and buffer layer on device performance

The absorber layer and buffer layer thickness is a very important parameter while determining the performance of a solar cell. The effect

of absorber layer thickness on the different solar cell parameters like open circuit voltage ( $V_{oc}$ ), short circuit current ( $I_{sc}$ ), fill factor (FF) and efficiency ( $\eta$ ) are studied thoroughly. For the simulation study, the thickness of absorber is varied from  $0.5 \mu\text{m}$  to  $4.0 \mu\text{m}$ . In this simulation study, the solar cell efficiency is determined by two factors, one is light absorption and another is carrier transportation. With a thin absorption layer, light absorption becomes a dominant factor as all the carriers can reach the corresponding electrode easily. When the absorber layer thickness is over a critical value, the light absorption is saturated and carrier transport becomes a deciding factor. Based on the interactions between these two factors, it is found from Fig. 2 (a) that with the increase in the thickness above  $2.5 \mu\text{m}$  and  $2 \mu\text{m}$  for  $\text{Sb}_2\text{S}_3$  and  $\text{Sb}_2\text{Se}_3$  solar cell, there is no significant change in the efficiency. The obtained thickness values are in good agreement with the experimental results obtained by other researchers [31–33]. If the thickness of the absorber layer is less, it can not absorb the total incoming light which leads to low efficiency. Similarly when the thickness is more than the optimum value, the travel path for the photo-generated carriers are long enough which is actually responsible for more recombination of generated carriers. Though the short circuit current for both the solar cell are getting saturated after a certain thickness value ( $1.5 \mu\text{m}$ – $2.0 \mu\text{m}$ ) but the open circuit voltage for  $\text{Sb}_2\text{S}_3$  is continuously varying with the increase in absorber layer thickness. With the increase in absorber layer thickness, there is an increase in the carrier recombination rate in comparison with the carrier generation rate, which leads to the saturation of  $J_{sc}$  when the thickness increases. It can also be seen from Fig. 2 (c) that the change in

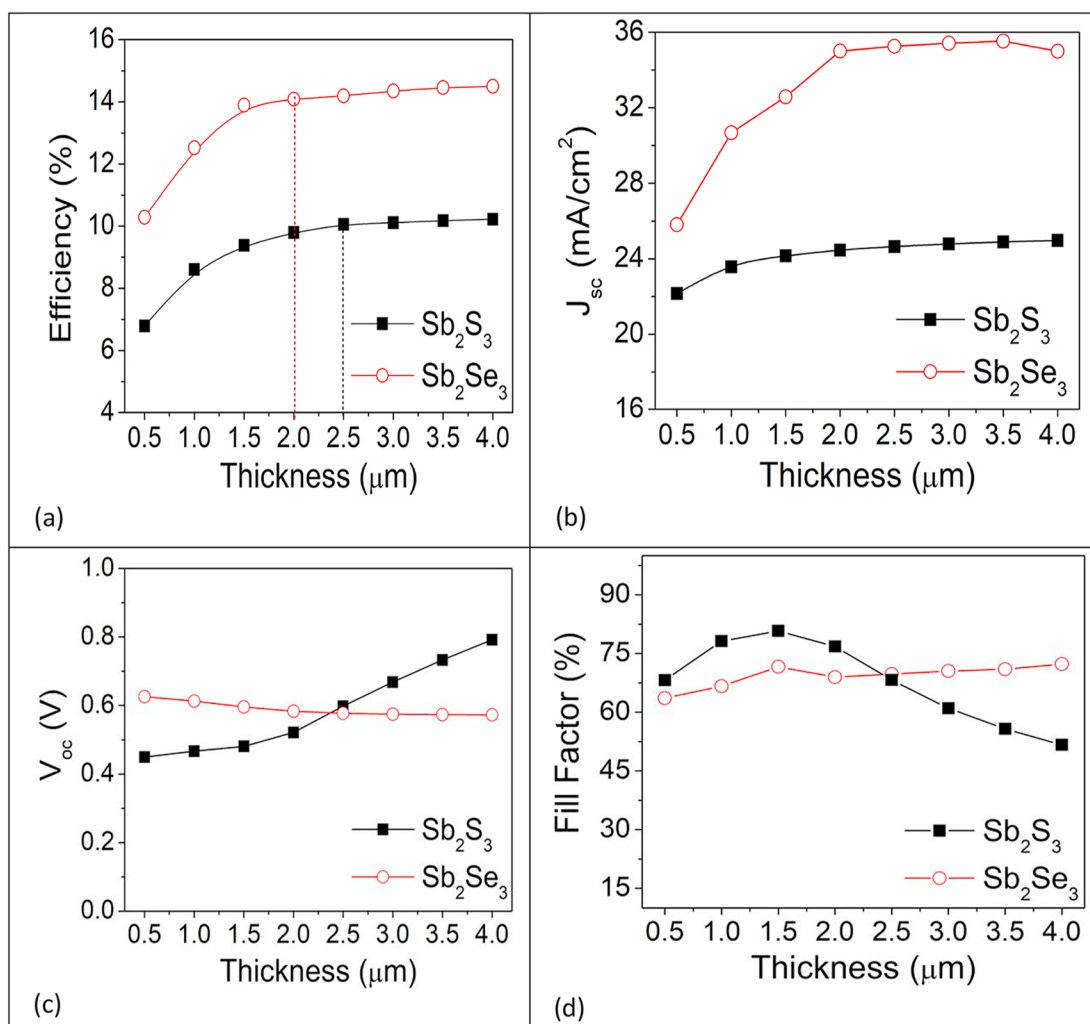


Fig. 2. Effect of the thickness of the absorber layer on the performance parameters of  $\text{Sb}_2\text{S}_3$  and  $\text{Sb}_2\text{Se}_3$  based solar cell.

$V_{oc}$  is almost constant for the lower range of thickness variation i.e. up to 2.5  $\mu\text{m}$  but after that a ramp type increase of  $V_{oc}$  is observed. This increase is due to the effective enhancement of the hole mobility of the  $\text{Sb}_2\text{S}_3$  layer which is more than the  $\text{Sb}_2\text{Se}_3$  as given in Table 1. The fill factor, as shown in Fig. 2 (d), for  $\text{Sb}_2\text{S}_3$  and  $\text{Sb}_2\text{Se}_3$  start increasing with the increase in the absorber layer thickness but at higher thicknesses, above 2.5  $\mu\text{m}$ , it starts decreasing for  $\text{Sb}_2\text{S}_3$  solar cell. With the increase in the thickness of absorber layer, the internal resistance is increased. This increase in the resistance enhanced the depletion which in turn reduces the fill factor [34].

To optimize the thickness of buffer layer, the simulation study was performed with a thickness range of 0.02  $\mu\text{m}$  to 0.120  $\mu\text{m}$  as shown in Fig. 3. Firstly the efficiency starts increasing with the increase in buffer layer thickness and then starts decreasing. This is because of the fact that very thin buffer layer results in high leakage current whereas very thick buffer layers absorb more photons that can not reach to the  $\text{Sb}_2\text{S}_3$  or  $\text{Sb}_2\text{Se}_3$  absorber layer. It is clear that for both the absorber layer the optimum thickness for CdS buffer layer is coming in the range of 0.05  $\mu\text{m}$  to 0.06  $\mu\text{m}$  [Fig. 3 (a)]. The open circuit voltage ( $V_{oc}$ ) for  $\text{Sb}_2\text{Se}_3$  is almost constant and the same for  $\text{Sb}_2\text{S}_3$  is increasing in a steady manner with the increase in thickness as shown in Fig. 3 (b). The increase open circuit voltage may be due to splitting of quasi-fermi level across the p-n junction with the increase in thickness of buffer layer [35]. Short circuit current ( $I_{sc}$ ) for  $\text{Sb}_2\text{Se}_3$  based solar cell is increasing, and for  $\text{Sb}_2\text{S}_3$  based solar cell it is decreasing with the increase in the thickness of buffer layer thickness as depicted in Fig. 3 (c). The fill factor is showing a phenomenon like firstly it is increasing and then start decreasing as the

thickness of buffer layer is increasing. Fill factor represents characteristics of the maximum power output when it is connected with optimal load. During this simulation the optimized thickness value of absorber layer obtained in the previous section was considered. For both of these simulations the impact of radiative recombination and series and shunt resistance were not considered. The obtained optimum thickness of CdS is similar to the experimental data found by other researchers [36,37].

### 3.2. Effect of variation of the radiative recombination coefficient

Recombination is a general phenomenon and main detrimental factor in designing high efficiency solar cells. This recombination need to be in minimum level. Radiative recombination mainly dominates in direct bandgap semiconductors. In radiative recombination, the electron from conduction band recombines directly with a hole in the valence band and releases a photon having energy similar to the bandgap. The value of the recombination coefficient also depends on the atomic structure and carrier density [38]. This simulation study was performed for the radiative recombination in the range of  $10^{-1} \text{ cm}^3/\text{s}$  to  $10^{-17} \text{ cm}^3/\text{s}$ . The maximum efficiency is obtained with the radiative recombination less than  $10^{-4} \text{ cm}^3/\text{s}$  and  $10^{-8} \text{ cm}^3/\text{s}$  for  $\text{Sb}_2\text{S}_3$  and  $\text{Sb}_2\text{Se}_3$  solar cell respectively as shown in Fig. 4(a). The open circuit voltage ( $V_{oc}$ ), short circuit current ( $I_{sc}$ ) and fill factor (FF) is also changing with the change in the radiative recombination coefficient as shown if Fig. 4(b-d). For the above optimization, the optimized thickness of absorber layer and buffer layer was taken into consideration whereas the series and effect of series and shunt resistance was not considered.

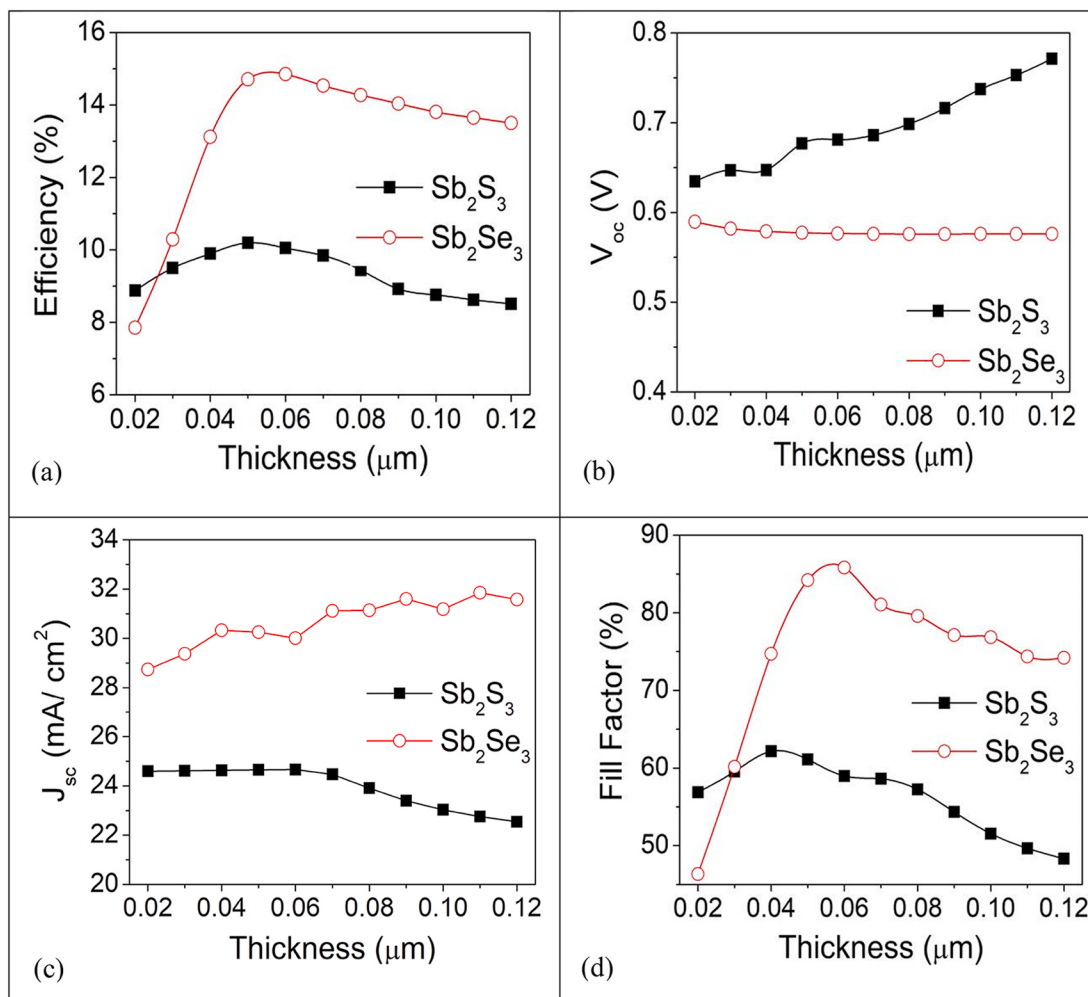
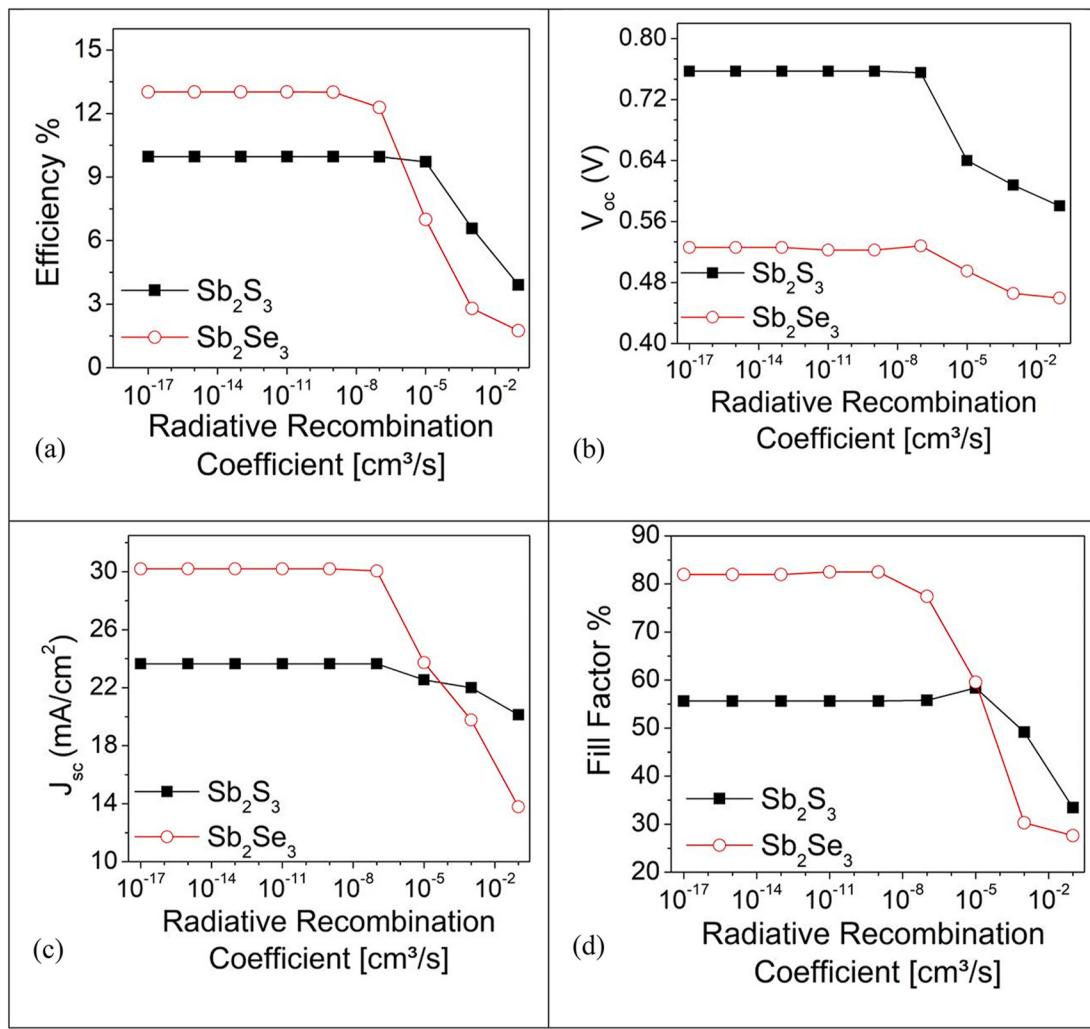


Fig. 3. Effect of thickness of buffer layer on the performance parameters of  $\text{Sb}_2\text{S}_3$  and  $\text{Sb}_2\text{Se}_3$  based solar cell.



**Fig. 4.** The effect of radiative recombination coefficient on the performance parameters of  $\text{Sb}_2\text{S}_3$  and  $\text{Sb}_2\text{Se}_3$  based solar cell.

### 3.3. Effect of variation in the concentration of defect density

Defect density is also an important factor which directly influences the performance parameters of solar cells. The photo-generated current is majorly generated by the absorber layer. Hence the increase in the defect density leads to an increase in carrier recombination which in turn affects the device efficiency. In this work to study the effect of the defect density, it is varied in the range of  $10^{10}$  cm<sup>-3</sup> to  $10^{20}$  cm<sup>-3</sup>. It is found that the defect density affects the output parameter of the solar cell in a significant manner as shown in Fig. 5. It is observed from Fig. 5 (a) that with the increase in defect density above  $10^{14}$  cm<sup>-3</sup> and  $10^{15}$  cm<sup>-3</sup> for the  $\text{Sb}_2\text{S}_3$  and  $\text{Sb}_2\text{Se}_3$  solar cell respectively the efficiency starts decreasing. Choi et al. [14] and chen et al. [39] reported the values of defect density which are in good agreement with the values obtained during the simulation. The open circuit voltage and short circuit current for  $\text{Sb}_2\text{S}_3$  decreases with the high values of defect density as shown in Fig. 5(b–c). The fill factor is showing the same trend for both the  $\text{Sb}_2\text{S}_3$  and  $\text{Sb}_2\text{Se}_3$  based solar cell as shown in Fig. 5 (d). However, the fill factor for  $\text{Sb}_2\text{Se}_3$  is more than  $\text{Sb}_2\text{S}_3$  for all the values of defect density. The increase in the defect density, carrier recombination rate increases which in turn decrease the carrier lifetime and diffusion length. So the overall performance of the device decreases [40]. As per other research studies, by precise controlling of deposition parameters,  $\text{Sb}_2\text{Se}_3$  films can grow along (0 0 1) direction which is perpendicular to p-n junction interface. This can reduce the defect density leading to achieve better efficiency [7].

### 3.4. Effect of change in the series and shunt resistance on device performance

Series and Shunt resistance play a very significant role on the performance of solar cell parameters. These parameters also determine the junction characteristics and its effect on the device performance. To determine the effect of series and shunt resistance, all other optimized parameters of the previous section were kept fixed at its optimum value. For this simulation study the series resistance ( $R_s$ ) and shunt resistance ( $R_{sh}$ ) were varied in the range of 1–28 Ω·cm<sup>2</sup> and 100–1500 Ω·cm<sup>2</sup> respectively. The effect of series and shunt resistance on the performance of solar cell parameters are shown in Fig. 6. It is found that the series and shunt resistance have strong influence on the efficiency of solar cells as in Fig. 6 (a) and 6 (e). The open circuit voltage ( $V_{oc}$ ) is more dependent of lower values of shunt resistance than series resistance whereas the short circuit current ( $I_{sc}$ ) is sensitive to the higher values of series resistance than the shunt resistance. The fill factor is also varying with the change in the series resistance. To study the impact of series and shunt resistance, the other parameters like absorber and buffer layer thickness, radiative recombination coefficient and defect density were kept at its optimum value as derived in the earlier sections. It is noted from experimental reports that the value of  $R_s$  and  $R_{sh}$  of  $\text{Sb}_2\text{S}_3$  and  $\text{Sb}_2\text{Se}_3$  based solar cell devices are in the range of 4.71–40 Ω·cm<sup>2</sup> and 49.9–856.35 Ω·cm<sup>2</sup> [41–44]. In this work the optimal value for  $R_s$  and  $R_{sh}$  of  $\text{Sb}_2\text{S}_3$  and  $\text{Sb}_2\text{Se}_3$  based solar cell devices are coming in the range of 3–5 Ω·cm<sup>2</sup> and 300–450 Ω·cm<sup>2</sup>.

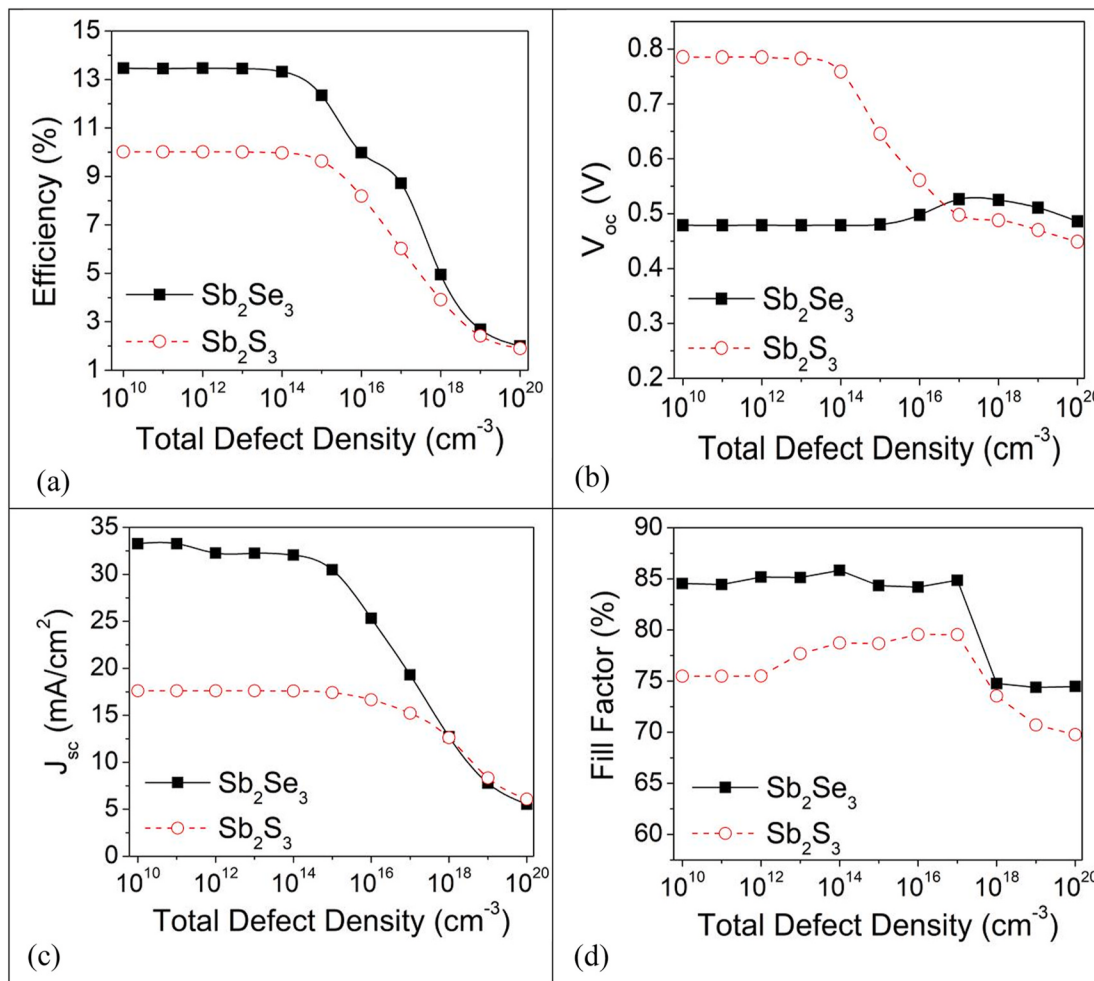


**Fig. 5.** The effect of defect density on the performance parameters of  $\text{Sb}_2\text{S}_3$  and  $\text{Sb}_2\text{Se}_3$  based solar cell.

### 3.5. Effect of the variation in the concentration of shallow acceptor density

Acceptor density plays a vital role in improving the efficiency of a solar cell. In the simulation study, the range of acceptor density was varied from  $10^{13}$   $\text{cm}^{-3}$  to  $10^{18}$   $\text{cm}^{-3}$ . It is found from Fig. 7 (a) that the maximum efficiency is obtained for acceptor density above  $10^{14}$   $\text{cm}^{-3}$  and  $10^{15}$   $\text{cm}^{-3}$  for  $\text{Sb}_2\text{Se}_3$  and  $\text{Sb}_2\text{S}_3$  based solar cell which is in accordance with the results obtained by Lin et al. [45] and Jiménez et al. [46]. This analysis reveals that the proper doping of absorber layer produce higher efficiency.

### 3.6. Effect of back contact work function on the device performance

The work function of the back contact also plays a vital role w.r.t. the enhancement of the efficiency of a solar cell. Several researchers have fabricated  $\text{Sb}_2\text{S}_3$  or  $\text{Sb}_2\text{Se}_3$  based solar cell devices having different metals as back contact like Mo [47], Al [48], Ag [49], Au [50], Pt [32]. Depending on the work function of the back contact, it will become a Schottky or ohmic one. In our simulation work we have varied the work function from 4.2 eV to 5.4 eV to study the effect of back contact on the performance of solar cell. In the initial steps, the efficiency is increasing with the increase in work function but it is found that after 5 eV the efficiency is becoming almost constant for the  $\text{Sb}_2\text{S}_3$  and  $\text{Sb}_2\text{Se}_3$  based solar cells as shown if Fig. 7 (b). In order to realize better efficiency of  $\text{Sb}_2\text{S}_3$  or  $\text{Sb}_2\text{Se}_3$  based solar cell, it is essential to choose an appropriate metal electrode. The obtained result is similar as reported by other

researchers [40,45].

The optimized device parameters for the  $\text{Sb}_2\text{S}_3$  and  $\text{Sb}_2\text{Se}_3$  based solar cell is shown in Table 2. The final I-V curve under optimized condition is shown in Fig. 8. The maximum efficiency obtained is 9.51% and 12.62% for  $\text{Sb}_2\text{S}_3$  and  $\text{Sb}_2\text{Se}_3$  based solar cell respectively.

The reported device parameters for  $\text{Sb}_2\text{S}_3$  and  $\text{Sb}_2\text{Se}_3$  based solar cell having the similar device structure as reported in this work with good efficiency is shown in Table 3 for a comparative analysis.

In the second stage of study, previously determined optimal parameters are used for the device structure. This study was taken up for better understanding of the insights of the device structure and to understand the shortcomings of  $\text{Sb}_2\text{S}_3$  and  $\text{Sb}_2\text{Se}_3$  based solar cells.

### 3.7. The carrier generation rate and built-in electric field of the optimized device

The variation of built-in electric field for  $\text{Sb}_2\text{S}_3$  and  $\text{Sb}_2\text{Se}_3$  based solar cells is shown in Fig. 9. According to Anderson model [56],

$$V_d = V_{d1} + V_{d2} = E_{g2} - \delta_{p2} - \delta_{n1} + \Delta E_c = E_{g1} - \delta_{p2} - \delta_{n1} - \Delta E_v \quad (4)$$

$$\Delta E_c = e(\chi_2 - \chi_1) \quad (5)$$

$$\Delta E_v = E_{g1} - E_{g2} - e(\chi_2 - \chi_1)$$

$V_d$  is the diffusion voltage in a p-type hetero-junction which is proportional to the electric field.

$V_{d1}$  and  $V_{d2}$  are the diffusion potentials in each region.

It is found from Fig. 9 that the generated electric field is more for

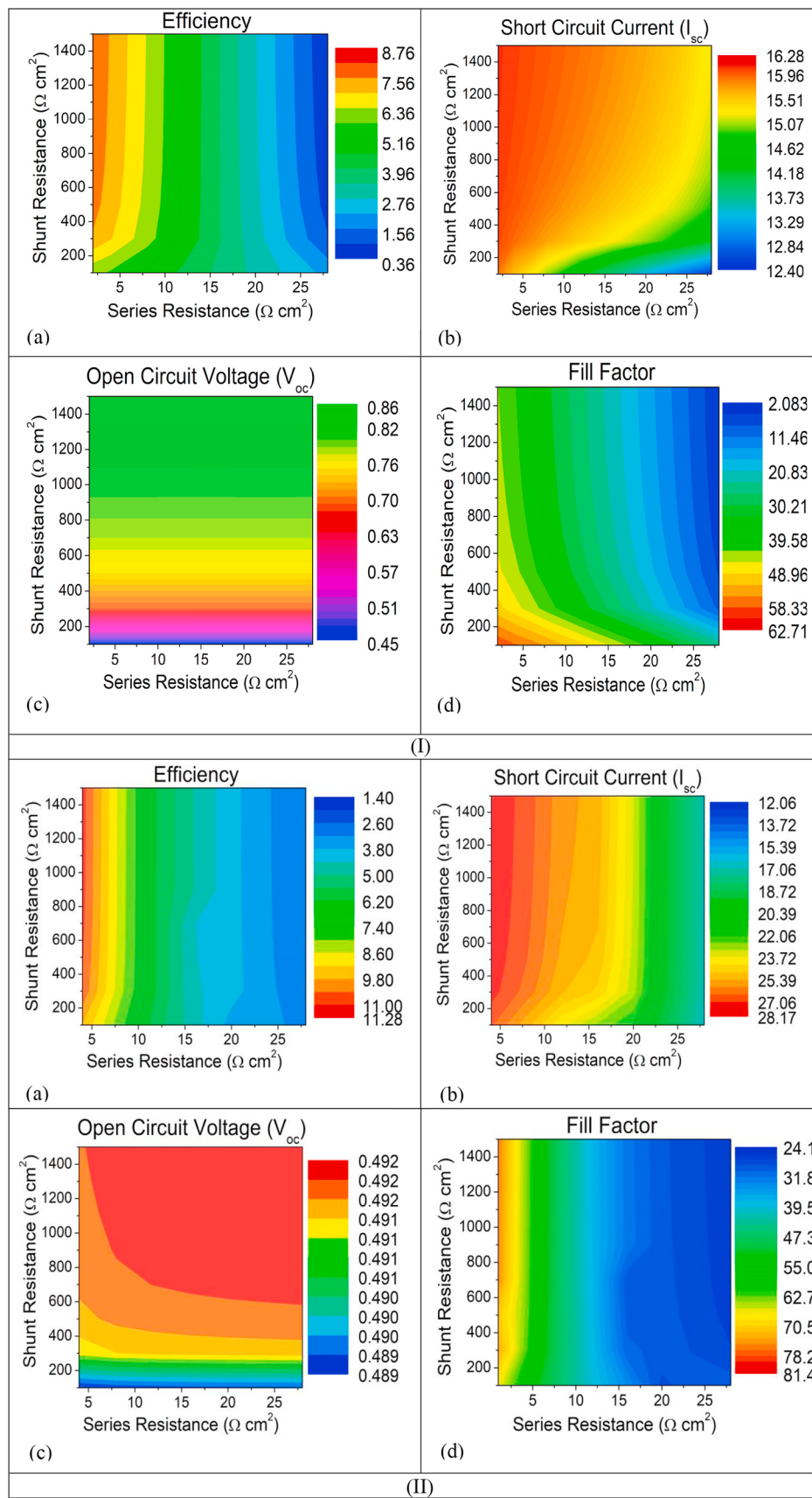


**Fig. 6.** The effect of series and shunt resistance on the performance parameters of (I) Sb<sub>2</sub>S<sub>3</sub> and (II) Sb<sub>2</sub>Se<sub>3</sub> based solar cell.

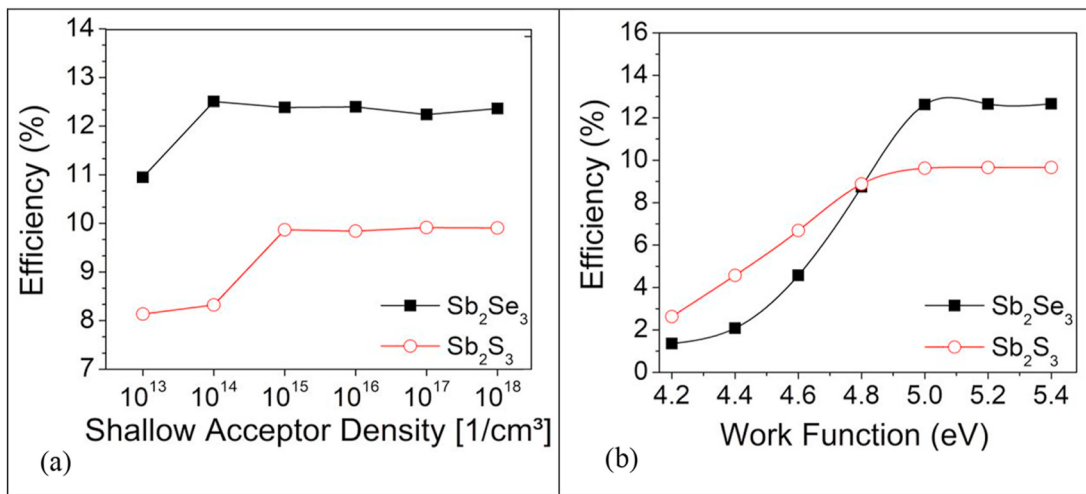


Fig. 7. The effect of (a) shallow acceptor density and (b) work function of back contact on the efficiency of Sb<sub>2</sub>S<sub>3</sub> and Sb<sub>2</sub>Se<sub>3</sub> based solar cell.

**Table 2**  
Optimized device parameter for the Sb<sub>2</sub>S<sub>3</sub> and Sb<sub>2</sub>Se<sub>3</sub> based solar cell.

Optimized Parameter	Sb <sub>2</sub> S <sub>3</sub>	Sb <sub>2</sub> Se <sub>3</sub>
Absorber layer and buffer layer thickness	2.5 μm	2 μm
Buffer layer thickness	0.05 μ - 0.06 μm	0.05 μm-0.06 μm
Radiative recombination coefficient	Less than 10 <sup>-4</sup> cm <sup>3</sup> /s	Less than 10 <sup>-8</sup> cm <sup>3</sup> /s
Defect density	Above 10 <sup>14</sup> cm <sup>-3</sup>	Above 10 <sup>15</sup> cm <sup>-3</sup>
Series and Shunt Resistance	R <sub>s</sub> = 3 - 5 Ω·cm <sup>2</sup> , R <sub>sh</sub> = 300 - 450 Ω·cm <sup>2</sup>	R <sub>s</sub> = 3 - 5 Ω·cm <sup>2</sup> , R <sub>sh</sub> = 300 - 450 Ω·cm <sup>2</sup>
Shallow Acceptor density	Above 10 <sup>14</sup> cm <sup>-3</sup>	Above 10 <sup>15</sup> cm <sup>-3</sup>
Back contact work function	5 eV	5 eV
Efficiency	9.51%	12.62%

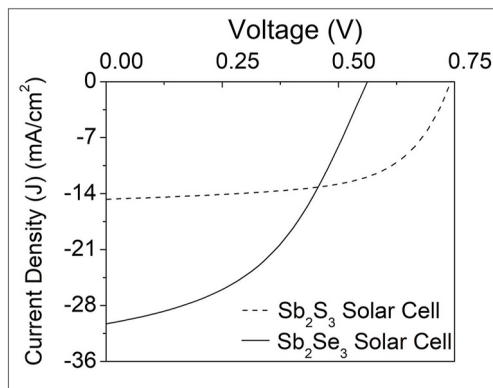


Fig. 8. The final I-V curve under optimized condition for Sb<sub>2</sub>S<sub>3</sub> and Sb<sub>2</sub>Se<sub>3</sub> based solar cells.

Sb<sub>2</sub>Se<sub>3</sub>/CdS than Sb<sub>2</sub>S<sub>3</sub>/CdS interface. This is because of the bandgap and work function gradient is more for Sb<sub>2</sub>Se<sub>3</sub> than Sb<sub>2</sub>S<sub>3</sub> with CdS. It is found that there is a strong value of electric field at the p-n junction but drops rapidly as we go inside the Sb<sub>2</sub>S<sub>3</sub> or Sb<sub>2</sub>Se<sub>3</sub> absorber layer. The built-in electric field enhances with the increase of the separation and transportation of photon-generated carriers [57].

The carrier generation and recombination rate for both the Sb<sub>2</sub>S<sub>3</sub> and Sb<sub>2</sub>Se<sub>3</sub> based solar cell is shown in Fig. 10. It can be seen from Fig. 10 that carrier generation and recombination rate for Sb<sub>2</sub>Se<sub>3</sub> based solar cell is higher than Sb<sub>2</sub>S<sub>3</sub> based solar cell. This is expected as Sb<sub>2</sub>Se<sub>3</sub> based solar cell has better J<sub>sc</sub> and PCE in comparison with Sb<sub>2</sub>S<sub>3</sub> based solar

**Table 3**

Comparison of efficiency and device parameters for Sb<sub>2</sub>S<sub>3</sub> and Sb<sub>2</sub>Se<sub>3</sub> based solar cell reported in literature compared with this work.

Device Structure	Efficiency (%)	J <sub>sc</sub> (mA/cm <sup>2</sup> )	V <sub>oc</sub> (mV)	FF (%)
<b>Reported experimental work</b>				
<b>Sb<sub>2</sub>S<sub>3</sub> based solar cell</b>				
ITO/CdS/Sb <sub>2</sub> S <sub>3</sub> /Au (Yuan et al., 2016) [58]	3.5	10.8	710	45.5
FTO/CdS/Sb <sub>2</sub> S <sub>3</sub> /Au (Chen et al., 2017) [16]	3.02	10.92	588	46.77
FTO/CdS/Sb <sub>2</sub> S <sub>3</sub> /Au (K. Wang et al., 2018) [51]	2.20	9.14	540	47.48
SLG/Mo/Sb <sub>2</sub> S <sub>3</sub> /CdS/i-ZO/AZO/Ni: Al (G. Pan et al., 2019) [11]	1.29	5.96	574	37.78
<b>Sb<sub>2</sub>Se<sub>3</sub> based solar cell</b>				
ITO/CdS/Sb <sub>2</sub> Se <sub>3</sub> /Au (Wen et al., 2018) [50]	7.6	29.9	420	60.4
ITO/CdS/Sb <sub>2</sub> Se <sub>3</sub> /Au (X. Hu et al., 2019) [52]	5.91	27.93	379	55.6
Mo/Sb <sub>2</sub> Se <sub>3</sub> /CdS/ITO/Ag (R. Tang et al., 2019) [53]	2.1	16.79	343	35.3
SLG/Mo/Sb <sub>2</sub> Se <sub>3</sub> /CdS/ZnO/ITO (Tiwari et al., 2020) [47]	4.34	19.8	386	56.7
SLG/Mo/Sb <sub>2</sub> Se <sub>3</sub> /CdS/ZnO/ITO/Ag (Liu et al., 2020) [54]	4.22	18.4	454	50.6
<b>Reported simulated work</b>				
<b>Sb<sub>2</sub>S<sub>3</sub> based solar cell</b>				
AZO/ZnO/CdS/Sb <sub>2</sub> S <sub>3</sub> /Au (Courel et al., 2019) [17]	20.6	20.15	1230	83.1
CdS/Sb <sub>2</sub> S <sub>3</sub> /Au (M.T. Islam and A.K. Thakur, 2020) [30]	18.52	24.44	948	79.96
FTO/ZnS/Sb <sub>2</sub> S <sub>3</sub> /Cu <sub>2</sub> O/Au (Xiao et al., 2020) [55]	16.65	23.73	970	72.32
<b>Sb<sub>2</sub>Se<sub>3</sub> based solar cell</b>				
FTO/CdS/Sb <sub>2</sub> Se <sub>3</sub> /Au (Lin et al., 2018) [45]	11.52	38.15	410	74.08
Mo/MoS <sub>2</sub> /Sb <sub>2</sub> Se <sub>3</sub> /TiO <sub>2</sub> /CdS/ZnO/ZnO:Al (Gharibshahian et al., 2020) [24]	9.17	32.56	400	70.3
<b>This simulated work</b>				
Mo/Sb <sub>2</sub> S <sub>3</sub> /CdS/i-ZnO/ZnO:Al/metal contact	9.51	15.98	723	83.23
Mo/Sb <sub>2</sub> Se <sub>3</sub> /CdS/i-ZnO/ZnO:Al/metal contact	12.62	31.79	560	70.81

cell. The defect states present inside the absorber layer are responsible for the reduction in the electron-hole recombination. Due to which energy states are created and affect the electron-hole recombination profile inside the solar cell device [27]. The generated electron and hole

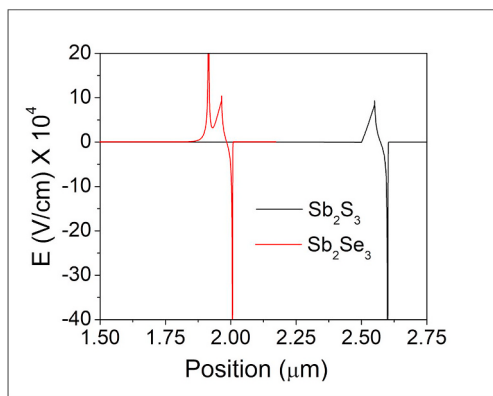


**Fig. 9.** The variation of built-in electric field for  $\text{Sb}_2\text{S}_3$  and  $\text{Sb}_2\text{Se}_3$  based solar cells.

pair cannot reach to the space charge region during their life span and ends up with recombination of the carriers due to the potential barrier present at the interface of  $\text{Sb}_2\text{Se}_3/\text{CdS}$  interface as shown in Fig. 11.

### 3.8. Capacitance ( $C$ ) – voltage ( $V$ ) characteristics of the optimized device

Capacitance-voltage study for the  $\text{Sb}_2\text{S}_3$  and  $\text{Sb}_2\text{Se}_3$  based solar cell was carried out to reveal more basic properties of the device structure.

Doping density and built-in potential are the basic two parameters derived from the capacitance-voltage characteristics from the following two relations [58],

$$\frac{1}{C^2} = \frac{2}{qN_a\epsilon_0\epsilon_s A^2}(V_{bi} - V) \quad (6)$$

$$N_a = \frac{2}{q\epsilon_0\epsilon_s A^2} \left[ \frac{d}{dv} \left( \frac{1}{C^2} \right) \right]$$

Where  $N_a$  = doping density ( $1/\text{cm}^3$ ),  $q$  = the charge of an electron ( $1.6 \times 10^{-19} \text{ C}$ ),  $\epsilon_0$  = permittivity of the free space ( $8.85 \times 10^{-14} \text{ F/cm}$ ),  $\epsilon_s$  = dielectric constant (as per Table 1),  $A$  = area of the cell ( $\text{cm}^2$ ),  $C$  = measured capacitance, and  $V$  = applied potential.

From the above two equations the built-in potential ( $V_{bi}$ ) and the doping density is calculated from the intercept and slope of the line in  $1/C^2$  vs.  $V$  plot as shown in Fig. 12. The  $V_{bi}$  is 0.71 V for  $\text{Sb}_2\text{S}_3$  and 0.49 V for  $\text{Sb}_2\text{Se}_3$  based solar cell. It is obvious as larger  $V_{bi}$  indicates an improved driving force for charge carriers separation which is responsible for improved  $V_{oc}$  for  $\text{Sb}_2\text{S}_3$  based solar cell [59]. The obtained built in potential value is coming in accordance with the values reported by other researchers [42,60].

The doping density ( $N_a$ ) calculated from the above equation is found to be  $5.69 \times 10^{15} \text{ cm}^{-3}$  and  $5.97 \times 10^{13} \text{ cm}^{-3}$  for  $\text{Sb}_2\text{S}_3$  and  $\text{Sb}_2\text{Se}_3$  based solar cell respectively. These values are very close to the carrier (hole)

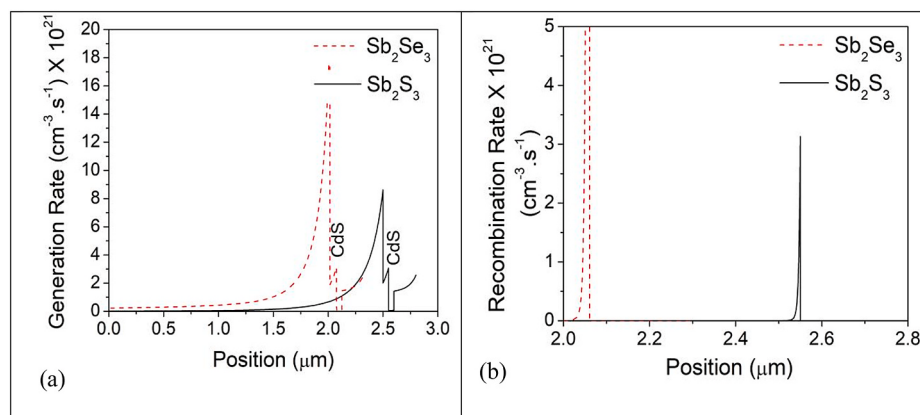


**Fig. 10.** The variation of generation and recombination rate for  $\text{Sb}_2\text{S}_3$  and  $\text{Sb}_2\text{Se}_3$  based solar cells.

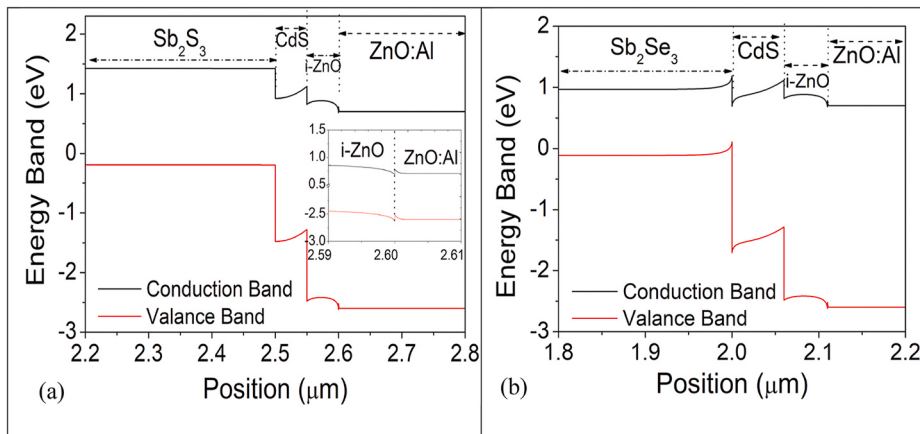


**Fig. 11.** Energy band gap diagram of the simulated (a)  $\text{Sb}_2\text{S}_3$  and (b)  $\text{Sb}_2\text{Se}_3$  based solar cells.

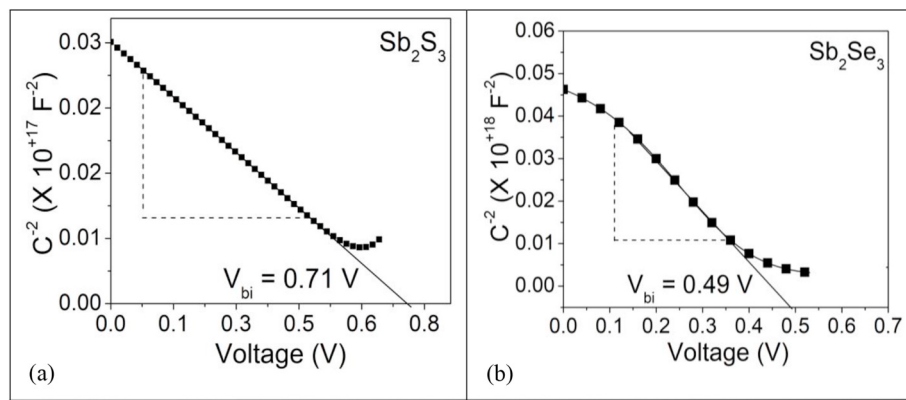


**Fig. 12.**  $1/C^2$  vs.  $V$  plot obtained for the simulated (a)  $\text{Sb}_2\text{S}_3$  and (b)  $\text{Sb}_2\text{Se}_3$  based solar cells.

density of the  $\text{Sb}_2\text{S}_3$  and  $\text{Sb}_2\text{Se}_3$  material taken for simulation (ref. Table 1).

With the obtained values of  $V_{bi}$  and  $N_a$ , the depletion width ( $W_d$ ) was calculated using the following relation [61],

$$W_d = \left( \frac{2\varepsilon_0 \varepsilon_s V_{bi}}{qN_a} \right)^{\frac{1}{2}} \quad (7)$$

The depletion width obtained is  $0.31 \mu\text{m}$  and  $0.29 \mu\text{m}$  for  $\text{Sb}_2\text{S}_3$  and  $\text{Sb}_2\text{Se}_3$  based solar cell respectively.

The carrier diffusion length was also estimated from the following relation,

$$L_n \sim \sqrt{D_n \tau} = \sqrt{\mu_n \frac{kT}{q} \tau} \quad (8)$$

Where,  $D_n$  is the diffusivity of the electrons,  $\mu_n$  is the electron mobility,  $\tau$  is the minority carrier lifetime and  $kT/q$  is the thermal voltage at room temperature (25.85 mV). After some value estimation, the carrier diffusion length found to be  $0.45 \mu\text{m}$  and  $0.56 \mu\text{m}$  for  $\text{Sb}_2\text{S}_3$  and  $\text{Sb}_2\text{Se}_3$  based solar cell. This distance is the average one, which an electron can travel towards the edge of space charge region before recombination.

So, after getting the values of depletion width and carrier diffusion length, the active thickness contributing to the photo-current can be written as,  $L_p = L_n + W_d$ , which is coming  $0.80 \mu\text{m}$  and  $0.77 \mu\text{m}$  for  $\text{Sb}_2\text{S}_3$  and  $\text{Sb}_2\text{Se}_3$  based solar cell.

#### 4. Conclusion

In this work,  $\text{Mo}/(\text{Sb}_2\text{S}_3 \text{ or } \text{Sb}_2\text{Se}_3)/\text{CdS}/i\text{-ZnO}/\text{ZnO:Al}$  solar cell were modeled and simulated using SCAPS-1D software to get the optimized device parameters which will help the researchers to obtain better photo conversion efficiency. The third-generation solar cell is optimized for various controllable parameters that affect the performance like thickness, recombination, defect and acceptor density, series and shunt resistance, work function of back contact within the experimentally permissible ranges. It is found from results that the thickness of the absorber vis-a-vis buffer layer have a large impact on the efficiency and other parameters of the solar cell. The thickness of the absorber layer is optimized within the range of  $2.0 \mu\text{m}$  to  $2.5 \mu\text{m}$  and the buffer layer thickness is optimized within the range of  $50 \text{ nm}$  to  $60 \text{ nm}$ . The simulated results also emphasized the importance in controlling the radiative recombination, shallow acceptor and defect density to get the optimum performance for the  $\text{Sb}_2\text{S}_3$  and  $\text{Sb}_2\text{Se}_3$  based solar cell. All these optimized parameters can be obtained by controlling the fabrication

methods. After optimizing all the above parameters the maximum efficiency obtained is 9.51% and 12.62% for the  $\text{Sb}_2\text{S}_3$  and  $\text{Sb}_2\text{Se}_3$  solar cells respectively. The junction characteristics for both the solar cells were also studied using in-built electric field, carrier generation and recombination rate, built-in potential, depletion width and diffusion length. It is found that the in-built electric field, carrier generation and recombination rate is more for  $\text{Sb}_2\text{Se}_3$  as compared to  $\text{Sb}_2\text{S}_3$  based solar cell. Also the built-in potential and depletion width for  $\text{Sb}_2\text{S}_3$  ( $0.91 \text{ V}$  and  $0.35 \mu\text{m}$ ) is more than  $\text{Sb}_2\text{Se}_3$  ( $0.25 \text{ V}$  and  $0.21 \mu\text{m}$ ) based solar cell. This report based on the simulation study and optimized parameters will help the researchers to fabricate higher efficiency  $\text{Sb}_2\text{S}_3$  and  $\text{Sb}_2\text{Se}_3$  based earth abundant, non-toxic third generation solar cells.

#### CRediT authorship contribution statement

**Arindam Basak:** Investigation, Visualization, Formal analysis, Writing – original draft, preparation, Resources, Writing and Editing.  
**Udai P. Singh:** Conceptualization, Reviewing, Supervision.

#### Declaration of competing interest

The authors declare that they have no known competing financial interests or personal relationships that could have appeared to influence the work reported in this paper.

#### Acknowledgement

The authors wish to thank the developers of SCAPS at the University of Gent for making their software package publicly available free of charge. The authors also like to acknowledge the financial support from DST-SERB under grant number EMR/2017/002196.

#### References

- [1] M.A. Green, Y. Hishikawa, E.D. Dunlop, D.H. Levi, J. Hohl-Ebinger, A.W.Y. Ho-Baillie, Solar cell efficiency tables (version 51), *Prog. Photovoltaics Res. Appl.* 26 (1) (2018) 3–12, <https://doi.org/10.1002/pip.2978>.
- [2] Charlotte Platzer-Björkman, Kesterite compound semiconductors for thin film solar cells, *Curr. Opin. Green Sustain. Chem.* 4 (2017) 84–90, <https://doi.org/10.1016/j.cogsc.2017.02.010>.
- [3] P. Jackson, R. Wuerz, D. Hariskos, E. Lotter, W. Witte, M. Powalla, Effects of heavy alkali elements in  $\text{Cu}(\text{In},\text{Ga})\text{Se}_2$  solar cells with efficiencies up to 22.6%, *Phys. Status Solidi Rapid Res. Lett.* 10 (8) (2016) 583–586, <https://doi.org/10.1002/pssr.201600199>.
- [4] Arindam Basak, Himangshu Deka, Anup Mondal, Udai P. Singh, Impact of post-deposition annealing in  $\text{Cu}_2\text{SnS}_3$  thin film solar cells prepared by doctor blade

- method, Vacuum 156 (2018) 298–301, <https://doi.org/10.1016/j.vacuum.2018.07.049>.
- [5] Chao Chen, Weiqi Li, Ying Zhou, Cheng Chen, Miao Luo, Xinshe Liu, Kai Zeng, Bo Yang, Chuanwei Zhang, Junbo Han, Jiang Tang, Optical properties of amorphous and polycrystalline Sb<sub>2</sub>Se<sub>3</sub> thin films prepared by thermal evaporation, Appl. Phys. Lett. 107 (2015), <https://doi.org/10.1063/1.4927741>, 043905.
- [6] Jingting Luo, Wei Xiong, Guangxing Liang, Yike Liu, Haozhi Yang, Zhuanghao Zheng, Xianghua Zhang, Ping Fan, Shuo Chen, Fabrication of Sb<sub>2</sub>S<sub>3</sub> thin films by magnetron sputtering and post-sulfurization/selenization for substrate structured solar cells, J. Alloys Compd. (2020) 154235, <https://doi.org/10.1016/j.jallcom.2020.154235>.
- [7] Y. Zhou, L. Wang, S. Chen, S. Qin, X. Liu, J. Chen, D.-J. Xue, M. Luo, Y. Cao, Y. Cheng, E.H. Sargent, J. Tang, Thin-film Sb<sub>2</sub>Se<sub>3</sub> photovoltaics with oriented one-dimensional ribbons and benign grain boundaries, Nat. Photonics 9 (2015) 409–415, <https://doi.org/10.1038/nphoton.2015.78>.
- [8] U. Chalapathi, B. Poornaprkash, Chang-Hoi Ahn, Si-Hyun Park, Rapid growth of Sb<sub>2</sub>S<sub>3</sub> thin films by chemical bath deposition with ethylenediamine tetraacetic acid additive, Appl. Surf. Sci. 451 (2018) 272–279, <https://doi.org/10.1016/j.apsusc.2018.04.249>.
- [9] Changhao Ma, Huafei Guo, Xin Wang, Zhiwen Chen, Qingfei Cang, Xuguang Jia, Yan Li, Ningyi Yuan, Jannning Ding, Fabrication of Sb<sub>2</sub>Se<sub>3</sub> thin film solar cells by co-sputtering of Sb<sub>2</sub>Se<sub>3</sub> and Se targets, Sol. Energy 193 (2019) 275–282.
- [10] Leng Zhang, Kongping Wu, Yu Jing, Yongyi Yu, Yaowei Wei, Sb<sub>2</sub>Se<sub>3</sub> Films Fabricated by Thermal Evaporation and Post Annealing, Vacuum (2020) 109840, <https://doi.org/10.1016/j.vacuum.2020.109840>.
- [11] Guoxing Pan, Dongxiao Wang, Shoushuai Gao, Peng Gao, Qiang Sun, Xingjiang Liu, Zhiqiang Zhou, Yun Sun, Yi Zhang, Substrate structured Sb<sub>2</sub>S<sub>3</sub> thin film solar cells fabricated by rapid thermal evaporation method, Sol. Energy 182 (2019) 64–71, <https://doi.org/10.1016/j.solener.2019.02.014>.
- [12] Fatima Haidar, Annie Pradel, Yuan Chen, Marie-Christine Record, Deposition of Sb<sub>2</sub>Se<sub>3</sub> thin films on Pt substrate via electro-chemical atomic layer epitaxy (EC-ALE), J. Electroanal. Chem. 879 (2020) 114774, <https://doi.org/10.1016/j.jelechem.2020.114774>.
- [13] Z. Li, X. Liang, G. Li, H. Liu, H. Zhang, J. Guo, J. Chen, K. Shen, X. San, W. Yu, R.E. I. Schropp, Y. Mai, 9.2%-efficient core-shell structured antimony selenide nanorod array solar cells, Nat. Commun. 10 (1) (2019) 125, <https://doi.org/10.1038/s41467-018-07903-6>.
- [14] Y.C. Choi, D.U. Lee, J.H. Noh, E.K. Kim, S.I. Seok, Highly improved Sb<sub>2</sub>S<sub>3</sub> sensitized-inorganic–organic heterojunction solar cells and quantification of traps by deep-level transient spectroscopy, Adv. Funct. Mater. 24 (2014) 3587–3592, <https://doi.org/10.1002/adfm.201304238>.
- [15] P.K. Nayak, S. Mahesh, H.J. Snaith, Cahen D., photovoltaic solar cell technologies: analysing the state of the art, Nat. Rev. Mater. 4 (2019) 269–285, <https://doi.org/10.1038/s41578-019-0097-0>.
- [16] Chao Chen, Tang Jiang, Open-circuit voltage loss of antimony chalcogenide solar cells: status, origin and possible solution, ACS Energy Lett. 5 (7) (2020) 2294–2304, <https://doi.org/10.1021/acsenergylett.0c00940>.
- [17] Maykel Courel, Thalía Jiménez, A. Arce-Plaza, D. Seuret-Jiménez, J.P. Morán-Lázaro, F.J. Sánchez-Rodríguez, A theoretical study on Sb<sub>2</sub>S<sub>3</sub> solar cells: the path to overcome the efficiency barrier of 8%, Sol. Energy Mater. Sol. Cell. 201 (2019) 110123, <https://doi.org/10.1016/j.solmat.2019.110123>.
- [18] Fasial Baig, Yousaf Khattak, Ahmed Shuja, Kashif Riaz, Bernabé Soucase, Performance investigation of Sb<sub>2</sub>Se<sub>3</sub> based solar cell by device optimization, band offset engineering and Hole Transport Layer in SCAPS-1D, Curr. Appl. Phys. 20 (2020), <https://doi.org/10.1016/j.cap.2020.06.005>.
- [19] Lhoussayne Et-taya, Touria Ouslimane, Abdellah Benami, Numerical analysis of earth-abundant Cu<sub>2</sub>ZnSn(S<sub>x</sub>Se<sub>1-x</sub>)<sub>4</sub> solar cells based on Spectroscopic Ellipsometry results by using SCAPS-1D, Sol. Energy 201 (2020) 827–835, <https://doi.org/10.1016/j.solener.2020.03.070>.
- [20] Y.Z. Hamri, Y. Bourezig, M. Medles, M. Ameri, K. Toumi, I. Ameri, Y. Al-Douri, C. H. Voon, Improved efficiency of Cu(In,Ga)Se<sub>2</sub> thin film solar cells using a buffer layer alternative to CdS, Sol. Energy 178 (2019) 150–156, <https://doi.org/10.1016/j.solener.2018.12.023>.
- [21] A. Hima, N. Lakhdar, B. Benhaoua, A. Saadoune, I. Kemerchou, F. Rogti, An optimized perovskite solar cell designs for high conversion efficiency, Superlattice. Microst. 129 (2019) 240–246, <https://doi.org/10.1016/j.jpsmi.2019.04.007>.
- [22] S. Zandi, P. Saxena, N.E. Gorji, Numerical simulation of heat distribution in RGO-contacted perovskite solar cells using COMSOL, Sol. Energy 197 (2020) 105–110, <https://doi.org/10.1016/j.solener.2019.12.050>.
- [23] A. Bag, R. Radhakrishnan, R. Nekovei, R. Jayakumar, Effect of absorber layer, hole transport layer thicknesses, and its doping density on the performance of perovskite solar cells by device simulation, Sol. Energy 196 (2020) 177–182, <https://doi.org/10.1016/j.solener.2019.12.014>.
- [24] Iman Gharibshahian, Ali A. Orooji, Samaneh Sharbati, Towards high efficiency Cd-Free Sb<sub>2</sub>Se<sub>3</sub> solar cells by the band alignment optimization, Sol. Energy Mater. Sol. Cells 212 (2020) 110581, <https://doi.org/10.1016/j.solmat.2020.110581>.
- [25] M. Burgelman, K. Decock, S. Khelifi, A. Abass, Advanced electrical simulation of thin film solar cells, Thin Solid Films 535 (2013) 296–301, <https://doi.org/10.1016/j.tsf.2012.10.032>.
- [26] Rajeshwari Garain, Arindam Basak, Udal P. Singh, Study of thickness and temperature dependence on the performance of SnS based solar cell by SCAPS-1D, Mater. Today: Proceedings 39 (2021) 1833–1837, <https://doi.org/10.1016/j.matpr.2020.06.185>. Part 5.
- [27] Manish Kumar, Abhishek Raj, Arvind Kumar, Avneesh Anshul, An optimized lead-free formamidinium Sn-based perovskite solar cell design for high power conversion efficiency by SCAPS simulation, Opt. Mater. 108 (2020) 110213, <https://doi.org/10.1016/j.optmat.2020.110213>.
- [28] Neelima Singh, Alpana Agarwal, Mohit Agarwal, Numerical simulation of highly efficient lead-free all-perovskite tandem solar cell, Sol. Energy 208 (2020) 399–410, <https://doi.org/10.1016/j.solener.2020.08.003>.
- [29] A. Benami, Effect of CZTS parameters on photovoltaic solar cell from numerical simulation, J. Energy Power Eng. 13 (2019) 32–36, <https://doi.org/10.17265/1934-8975/2019.01.003>.
- [30] M.T. Islam, A.K. Thakur, Two stage modelling of solar photovoltaic cells based on Sb<sub>2</sub>S<sub>3</sub> absorber with three distinct buffer combinations, Sol. Energy 202 (2020) 304–315, <https://doi.org/10.1016/j.solener.2020.03.058>.
- [31] O. Savadogo, K.C. Mandal, Low-cost technique for preparing n-Sb<sub>2</sub>S<sub>3</sub>/p-Si heterojunction solar cells, Appl. Phys. Lett. 63 (1993) 228–230, <https://doi.org/10.1063/1.110349>.
- [32] O. Savadogo, K.C. Mandal, Low cost Schottky barrier solar cells fabricated on CdSe and Sb<sub>2</sub>S<sub>3</sub> films chemically deposited with silicotungstic acid, J. Electrochem. Soc. 141 (1994) 2871, <https://doi.org/10.1149/1.2059248>.
- [33] Al Ahmed Sheikh Rashel, Sunny Adil, Sabrina Rahman, Performance enhancement of Sb<sub>2</sub>Se<sub>3</sub> solar cell using a back surface field layer: a numerical simulation approach, Sol. Energy Mater. Sol. Cell. 221 (2021) 110919, <https://doi.org/10.1016/j.solmat.2020.110919>.
- [34] G.M.W. Bissels, J.J. Schermer, M.A.H. Asselbergs, E.J. Haverkamp, P. Mulder, G. J. Bauhuis, E. Vlieg, Theoretical review of series resistance determination methods for solar cells, Sol. Energy Mater. Sol. Cells 130 (2014) 605–614, <https://doi.org/10.1016/j.solmat.2014.08.003>.
- [35] Arindam Basak, Anup Mondal, Udai P. Singh, Post-growth annealing effect on the performance of Cu<sub>2</sub>SnSe<sub>3</sub> solar cells, Mater. Res. Express 5 (2018) 105505, <https://doi.org/10.1088/2053-1591/aada00>.
- [36] Liping Guo, Baiyu Zhang, Shan Li, Qian Zhang, Michael Buettner, Li Lin, Xiaofeng Qian, Feng Yan, Scalable and efficient Sb<sub>2</sub>S<sub>3</sub> thin-film solar cells fabricated by close space sublimation, Apl. Mater. 7 (2019), <https://doi.org/10.1063/1.5090773>, 041105.
- [37] Ying Zhou, Li Yang, Jiajun Luo, Dengbing Li, Xinheng Liu, Chao Chen, Huaiying Song, Jingyuan Ma, Ding-Jiang Xue, Bo Yang, Tang Jiang, Buried homojunction in CdS/Sb<sub>2</sub>Se<sub>3</sub> thin film photovoltaics generated by interfacial diffusion, Appl. Phys. Lett. 111 (2017), <https://doi.org/10.1063/1.4991539>, 013901.
- [38] Xie Zhang, Jimmy-Xuan Shen, Wennie Wang, G. Chris, Walle Van de, First-principles analysis of radiative recombination in lead-halide perovskites, ACS Energy Lett. 3 (10) (2018) 2329–2334, <https://doi.org/10.1021/acsenergylett.8b01297>.
- [39] C. Chen, D.C. Bobela, Y. Yang, et al., Characterization of basic physical properties of Sb<sub>2</sub>Se<sub>3</sub> and its relevance for photovoltaics, Front. Optoelectron. 10 (2017) 18–30, <https://doi.org/10.1007/s12200-017-0702-z>.
- [40] Zhen-Qi Li, Ming Ni, Xiao-Dong Feng, Simulation of the Sb<sub>2</sub>Se<sub>3</sub> solar cell with a hole transport layer, Mater. Res. Express 7 (2020), <https://doi.org/10.1088/2053-1591/ab5fa7>, 016416.
- [41] M. Tamilselvan, A. Byregowda, C.-Y. Su, C.-J. Tseng, A.J. Bhattacharyya, Planar heterojunction solar cell employing a single-source precursor solution-processed Sb<sub>2</sub>S<sub>3</sub> thin film as the light absorber, ACS Omega 4 (2019) 11380–11387, <https://doi.org/10.1021/acsomega.9b01245>.
- [42] Ke Yang, Bing Li, Guanggen Zeng, Effects of substrate temperature and SnO<sub>2</sub> high resistive layer on Sb<sub>2</sub>Se<sub>3</sub> thin film solar cells prepared by pulsed laser deposition, Sol. Energy Mater. Sol. Cells 208 (2020) 110381, <https://doi.org/10.1016/j.solmat.2019.110381>.
- [43] Qingfei Cang, Huafei Guo, Xuguang Jia, Huan Ning, Changhao Ma, Jiayi Zhang, Ningyi Yuan, Jannning Ding, Enhancement in the efficiency of Sb<sub>2</sub>Se<sub>3</sub> solar cells by adding low lattice mismatch Cu<sub>2</sub>Se<sub>2</sub> hole transport layer, Sol. Energy 199 (2020) 19–25, <https://doi.org/10.1016/j.solener.2020.02.008>.
- [44] C. Wu, C. Jiang, X. Wang, H. Ding, H. Ju, L. Zhang, T. Chen, C. Zhu, Interfacial engineering by indium-doped CdS for high efficiency solution processed Sb<sub>2</sub>(S<sub>1-x</sub>Se<sub>x</sub>)<sub>3</sub> solar cells, ACS Appl. Mater. Interfaces 11 (2019) 3207–3213, <https://doi.org/10.1021/acsami.8b18330>.
- [45] Ling-yan Lin, Lin-qin Jiang, Yu Qiu, Bao-dian Fan, Analysis of Sb<sub>2</sub>Se<sub>3</sub>/CdS based photovoltaic cell: a numerical simulation approach, J. Phys. Chem. Solid. 122 (2018) 19–24, <https://doi.org/10.1016/j.jpcs.2018.05.045>.
- [46] T. Jiménez, D. Seuret-Jiménez, O. Vigil-Galán, M. Basurto-Pensado, M. Courel, Sb<sub>2</sub>(S<sub>1-x</sub>Se<sub>x</sub>)<sub>3</sub> solar cells: the impact of radiative and non-radiative loss mechanisms, J. Phys. D 51 (2018) 435501, <https://doi.org/10.1088/1361-6463/aadea>.
- [47] Kunal J. Tiwari, Markus Neuschitzer, Moises Espíndola-Rodríguez, Yudiana Sanchez, Zacharie Jehl, Pedro Vidal-Fuentes, Edgardo Saucedo, Piraviperumal Malar, Efficient Sb<sub>2</sub>Se<sub>3</sub>/CdS planar heterojunction solar cells in substrate configuration with (hk0) oriented Sb<sub>2</sub>Se<sub>3</sub> thin films, Sol. Energy Mater. Sol. Cells 215 (2020) 110603, <https://doi.org/10.1016/j.solmat.2020.110603>.
- [48] Donglou Ren, Shuo Chen, Michel Cathelinraud, Guangxing Liang, Hongli Ma, Xianghua Zhang, Fundamental physical characterization of Sb<sub>2</sub>Se<sub>3</sub>-based quasi-homojunction thin film solar cells, ACS Appl. Mater. Interfaces 12 (27) (2020) 30572–30583, <https://doi.org/10.1021/acsami.0c08180>.
- [49] Guang-Xing Liang, Yan-Di Luo, Shuo Chen, Rong Tang, Zhuang-Hao Zheng, Xue-Jin Li, Xin-Sheng Liu, Yi-Ke Liu, Ying-Fen Li, Xing-Ye Chen, Zheng-Hua Su, Xiang-Hua Zhang, Hong-Li Ma, Ping Fan, Sputtered and selenized Sb<sub>2</sub>Se<sub>3</sub> thin-film solar cells with open-circuit voltage exceeding 500 mV, Nano Energy 73 (2020) 104806, <https://doi.org/10.1016/j.nanoen.2020.105105>.
- [50] X. Wen, C. Chen, S. Lu, K. Li, R. Kondrotas, Y. Zhao, W. Chen, L. Gao, C. Wang, J. Zhang, G. Niu, J. Tang, Vapor transport deposition of antimony selenide thin

- film solar cells with 7.6% efficiency, *Nat. Commun.* 9 (2018) 2179, <https://doi.org/10.1038/s41467-018-04634-6>.
- [51] K. Wang, J. Cheng, X. Yang, R. Hu, L. Fu, J. Huang, J. Yu, L. Li, Enhanced photovoltaic properties in  $Sb_2S_3$  planar heterojunction solar cell with a fast selenylation approach, *Nanoscale Res. Lett.* 13 (2018), <https://doi.org/10.1186/s11671-018-2651-x>.
- [52] Xiaobo Hu, Jiahua Tao, Youyang Wang, Juanjuan Xue, Guoent Weng, Chuanjun Zhang, Shaoqiang Chen, Ziqiang Zhu, Junhao Chu, 5.91%-efficient  $Sb_2Se_3$  solar cells with a radio-frequency magnetron-sputtered CdS buffer layer, *Appl. Mater. Today* 16 (2019) 367–374, <https://doi.org/10.1016/j.apmt.2019.06.001>.
- [53] Rong Tang, Xing-Ye Chen, Guang-Xing Liang, Zheng-Hua Su, Jing-ting Luo, Ping Fan, Magnetron sputtering deposition and selenization of  $Sb_2Se_3$  thin film for substrate  $Sb_2Se_3/CdS$  solar cells, *Surf. Coating. Technol.* 360 (2019) 68–72, <https://doi.org/10.1016/j.surcoat.2018.12.102>.
- [54] Xinsheng Liu, Yajun Qiao, Ya Liu, Jingling Liu, Erguang Jia, Songfeng Chang, Xingfen Shen, Shuang Li, Ke Cheng, Enhanced open circuit voltage of  $Sb_2Se_3/CdS$  solar cells by annealing Se-rich amorphous  $Sb_2Se_3$  films prepared via sputtering process, *Sol. Energy* 195 (2020) 697–702, <https://doi.org/10.1016/j.solener.2019.11.072>.
- [55] Youpeng Xiao, Huaiping Wang, Hai Kuang, Numerical simulation and performance optimization of  $Sb_2S_3$  solar cell with a hole transport layer, *Opt. Mater.* 108 (2020) 110414, <https://doi.org/10.1016/j.optmat.2020.110414>.
- [56] F. Belarbi, W. Rahal, D. Rached, S. benghabrit, M. Adnane, A comparative study of different buffer layers for CZTS solar cell using Scaps-1D simulation program, *Optik - Int. J. Light Electron Opt.* 216 (2020) 164743, <https://doi.org/10.1016/j.ijleo.2020.164743>.
- [57] S. Yuan, H. Deng, D. Dong, X. Yang, K. Qiao, C. Hu, Huaibing Song, Haisheng Song, Z. He, J. Tang, Efficient planar antimony sulfide thin film photovoltaics with large grain and preferential growth, *Sol. Energy Mater. Sol. Cells* 157 (2016) 887–893, <https://doi.org/10.1016/j.solmat.2016.07.050>.
- [58] S.K. Tripathi, M. Sharma, Analysis of the forward and reverse bias I-V and C-V characteristics on Al/PVA:n-PbSe polymer nanocomposites Schottky diode, *J. Appl. Phys.* 111 (2012), <https://doi.org/10.1063/1.3698773>, 074513.
- [59] Jian Han, Xingyu Pu, Hui Zhou, Cao Qi, Shuangjie Wang, Jiabao Yang, Junsong Zhao, Xuanhua Li, Multidentate anchoring through additive engineering for highly efficient  $Sb_2S_3$  planar thin film solar cells, *J. Mater. Sci. Technol.* 89 (2021) 36–44, <https://doi.org/10.1016/j.jmst.2021.01.078>.
- [60] C. Jiang, R. Tang, X. Wang, H. Ju, G. Chen, T. Chen, Alkali metals doping for high-performance planar heterojunction  $Sb_2S_3$  solar cells, *Sol. RRL* 3 (2019) 1800272, <https://doi.org/10.1002/solr.201800272>.
- [61] B. Shin, O. Gunawan, Y. Zhu, N.A. Bojarczuk, S.J. Chey, S. Guha, Thin film solar cell with 8.4% power conversion efficiency using an earth-abundant  $Cu_2ZnSnS_4$  absorber, *Prog. Photovoltaics Res. Appl.* 21 (2013) 72–76, <https://doi.org/10.1002/pip.1174>.